Semianalytical model for simulation of electronic properties of narrow-gap strained semiconductor quantum nanostructures

J. Even,* F. Doré, C. Cornet, and L. Pedesseau
FOTON-INSA Laboratory, UMR 6082 au CNRS, INSA de Rennes, 20 Avenue des Buttes de Coësmes, CS 14315, 35043 Rennes Cedex, France

(Received 9 July 2007; revised manuscript received 7 November 2007; published 6 February 2008)

A complete semianalytical model is proposed for the simulation of the electronic, mechanical, and piezoelectric properties of narrow-gap strained semiconductor quantum nanostructures. A transverse isotropic approximation for the strain and an axial approximation for the strained 8×8 Hamiltonian are proposed. It is applied extensively to the case of InAs/InP quantum dots (QDs). Symmetry analysis shows that there does exist a nonvanishing splitting on the electron P states due to the coupling with valence band. This splitting, which was not considered before, is found to be smaller in InAs/GaAs QD than in InAs/InP QD. Analytic expressions for the first and second order piezoelectric polarizations are used to evaluate the perturbation of electronic states.

DOI: 10.1103/PhysRevB.77.085305 PACS number(s): 73.21.La, 71.20.Nr, 78.20.Hp

I. INTRODUCTION

The eight-band $k\cdot p$ model of strained zinc-blende crystals[1] has now been extensively used to describe the electronic structure of III-V semiconductor nanostructures, especially at the Γ point ($k=0$) for interband direct transitions. Based on envelope function approximation, the eight-band $k\cdot p$ model is especially well adapted for studying small gaps materials, and the influence of deformations on interband coupling. The efficiency of this model has been demonstrated on various materials systems, such as In(Ga)As/GaAs,[2] InAs/InP,[3] or InAsSb/InP.[4] Some more complicated (but more precise) atomistic models have also been used to describe the fine electronic structure of such nanostructures.[5–7] In these studies, three effects are assumed to have an impact on fine electronic structure: (i) interfacial symmetry, (ii) atomistic strain, and (iii) piezoelectricity.

The eight-band $k\cdot p$ Hamiltonian for bulk strained materials is known[8] to exhibit a twofold degenerate spectrum related to a diagonalization into two 4×4 blocks, exhibiting a dependence on the k vector. A unitary transformation of this kind, but independent on the tranverse k vector, has been introduced to transform the 6×6 Hamiltonian in quantum wells into two 3×3 blocks[9] and more recently[10] to transform the 8×8 Hamiltonian (two 4×4 blocks) for type-II interband cascade lasers. The same approximation was used for cylindrical quantum wires (QWr).[11,12] The Hamiltonian is block diagonal with the use of a new basis. For the simulation of the electronic properties of quantum dots (QDs), the $k\cdot p$ method[2,3,13] is more or less a standard method although more elaborate theoretical schemes can be employed.[5–7] The strained-dependent 6×6 Hamiltonian for the valence band in $InP/In_{0.49}Ga_{0.51}P$ QD was simplified into an axially symmetric form in Ref. 14 We propose in the present work to extend these approaches to the 8×8 Hamiltonian in order to provide a fast and easy method to evaluate the electronic spectra of narrow-gap semiconductor QDs. Strain effects are taken carefully into account. A axial approximation is proposed for the strained part of the 8×8 Hamiltonian and applied to InAs/InP and InAs/GaAs QDs.

II. AXIAL APPROXIMATION

We will consider in this paper QD geometries corresponding to the $C_{\infty v}$ symmetry (rotational symmetry around the z [001] axis). The real calculation is performed in two-dimensional (2D) cylindrical coordinates $(\boldsymbol{r},z)$ on truncated cones of various heights. The chosen dimensions are 8.8 nm for the cone height and 35 nm for the diameter.[3] Our previous results on InAs/InP QD were obtained either using a complete three-dimensional (3D) eight-band $k\cdot p$ strained Hamiltonian[3] or a simple one-band $k\cdot p$ Hamiltonian with strain renormalized constants in 2D cylindrical coordinates.[15]

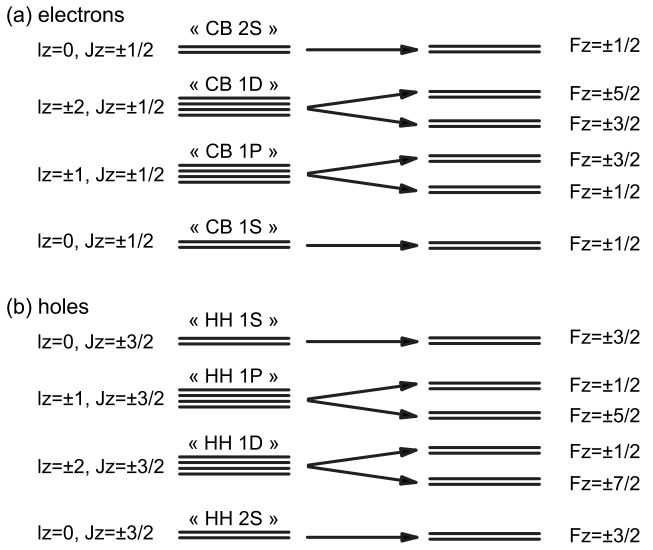

FIG. 1. Comparison between (a) CB and (b) valence band (VB) states close to the band gap in the one-band representation on the left and in the axial eight-band representation on the right. The CB and VB ground states are associated, respectively, with $\boldsymbol{F}_z=\pm1/2$ and $\boldsymbol{F}_z=\pm3/2$. The degeneracies of CB and VB first excited states in the one-band representation ("CB 1P" and "HH 1P") are lifted by the coupling to remote bands.

We may notice that InAs QD grown either on (100) or (311)*B* misoriented surface are interesting for applications purposes.[4,16] The present model is, however expected to be applied only to QD grown on (100) with cylindrical symmetry. InAs/GaAs QD are finally considered for comparison purposes.

We start from the 8×8 strained Hamiltonian for bulk materials given in Ref. 1 or 13.

$$\begin{pmatrix}
A & 0 & V^* & 0 & \sqrt{3}V & -\sqrt{2}U & -U & \sqrt{2}V^* \\
0 & A & -\sqrt{2}U & -\sqrt{3}V^* & 0 & -V & \sqrt{2}V & U \\
V & -\sqrt{2}U & -P+Q & -S^* & R & 0 & \sqrt{\frac{3}{2}}S & -\sqrt{2}Q \\
0 & -\sqrt{3}V & -S & -P-Q & 0 & R & -\sqrt{2}R & \frac{1}{\sqrt{2}}S \\
\sqrt{3}V^* & 0 & R^* & 0 & -P-Q & S^* & \frac{1}{\sqrt{2}}S^* & \sqrt{2}R^* \\
-\sqrt{2}U & -V^* & 0 & R^* & S & -P+Q & \sqrt{2}Q & \sqrt{\frac{3}{2}}S^* \\
-U & \sqrt{2}V^* & \sqrt{\frac{3}{2}}S^* & -\sqrt{2}R^* & \frac{1}{\sqrt{2}}S & \sqrt{2}Q & -P-\Delta & 0 \\
\sqrt{2}V & U & -\sqrt{2}Q & \frac{1}{\sqrt{2}}S^* & \sqrt{2}R & \sqrt{\frac{3}{2}}S & 0 & -P-\Delta
\end{pmatrix}.$$

When considering first the unstrained part of the Hamiltonian, the axial approximation is the same as for the 6×6 bulk Hamiltonian,[9,14]

$$R = -\sqrt{3}\frac{\hbar^2}{2m_0}[\gamma_2(k_x^2-k_y^2) - 2i\gamma_3 k_x k_y] \approx -\sqrt{3}\frac{\hbar^2}{2m_0}\bar{\gamma}k_-^2. \tag{1}$$

$$\boldsymbol{R}^* = -\sqrt{3}\frac{\hbar^2}{2\boldsymbol{m}_0}\boldsymbol{k}_+\bar{\boldsymbol{\gamma}}\boldsymbol{k}_+.$$

The other terms of the Hamiltonian can be expressed as a function of the $\boldsymbol{k}_z$ and $k_\pm=-ie^{\pm i\varphi}[(\partial/\partial r)\pm(i/r)(\partial/\partial\varphi)]$ operators, without any more approximations for $\boldsymbol{S}$, $\boldsymbol{P}$, and $\boldsymbol{Q}$.

$$S = \sqrt{3}\frac{\hbar^2}{2m_0}(k_-\gamma k_z + k_z\gamma k_-), \quad S^* = \sqrt{3}\frac{\hbar^2}{2m_0}(k_+\gamma k_z + k_z\gamma k_+),$$

$$P = -E_v - \frac{\hbar^2}{2m_0}\left(\frac{k_-\gamma_1 k_+ + k_+\gamma_1 k_-}{2} + k_z\gamma_1 k_z\right),$$

$$Q = -\frac{\hbar^2}{2m_0}\left(\frac{k_-\gamma_2 k_+ + k_+\gamma_2 k_-}{2} - 2k_z\gamma_2 k_z\right).$$

To extend the model used in Refs. 9 and 14 to the 8×8 QD Hamiltonian, we introduce

$$U = \frac{1}{2\sqrt{3}}\frac{\hbar^2}{2m_0}(P_o k_z + k_z P_o), \tag{2}$$

$$V = \frac{1}{2\sqrt{6}}\frac{\hbar^2}{2m_0}(P_o k_- + k_- P_o), \quad V^* = \frac{1}{2\sqrt{6}}\frac{\hbar^2}{2m_0}(P_o k_+ + k_+ P_o), \tag{3}$$

and

$$A = E_c + \frac{\hbar^2}{2m_0}\left(\frac{k_-k_+ + k_+k_-}{2} + k_z k_z\right), \tag{4}$$

By analogy to QWr,[11,12] it is straightforward to check that the 8×8 QD Hamiltonian is block diagonal in an $\boldsymbol{F}_z$ basis, where $\boldsymbol{F}_z=J_z+L_Z$ is the total angular momentum. Thus, $\boldsymbol{F}_z$ becomes a good quantum number (each block corresponds to one F_z value). The basis is constructed in a product form $|\boldsymbol{J},\boldsymbol{J}_z\rangle|\boldsymbol{L}_z=\boldsymbol{F}_z-\boldsymbol{J}_z\rangle$, where the first factor corresponds to the band-edge Bloch functions [the (u_1,u_2), (u_4,u_5), (u_3,u_6), and (u_7,u_8) bands are, respectively, related to the conduction band (CB), heavy holes (HH), light holes (LH), and split-off bands].[15] The second factor $|\boldsymbol{L}_z=\boldsymbol{F}_z-\boldsymbol{J}_z\rangle$ corresponds to the envelope functions adapted to the usual one-band cylindrical representation ($C_{\infty v}$ symmetry). $L_z=0,\pm1,\pm2,\ldots$ are related to the so-called $S,P,D,\ldots$ radial functions of this representation.[15] All monoelectronic states are a mixing of eight bands but we will still indicate, if possible, the most important component (for example, "CB 1-S" for the CB ground state). The boundary conditions are of Neuman type for the *S*-like radial functions (i.e., functions derivatives are equal to 0 for $r=0$, in the frame of a finite elements reso-

lution) and of the Dirichlet type for all the other radial functions (i.e., functions are equal to 0 for $r=0$, in the frame of a finite elements resolution).

This new basis is interesting for several reasons. The state degeneracy is automatically taken into account with $\boldsymbol{F}_z$ and $-\boldsymbol{F}_z$. It is also possible to obtain a schematic electronic spectrum, based only on symmetry considerations. Figure 1 is a comparison between the (a) CB and (b) valence band (VB) states close to the band gap in the one-band representation on the left and in the axial eight-band representation on the right. The CB ground state is mainly associated with $\boldsymbol{F}_z = \pm 1/2$ and to the u_1 or u_2 band-edge Bloch functions and the first S-like envelope functions. The VB ground state is "HH 1S" with $\boldsymbol{F}_z = \pm 3/2$. The electronic gap is then obtained after two separate calculations with $F_z = \pm 1/2$ and $\boldsymbol{F}_z = \pm 3/2$. Another important result of this symmetry analysis is that the degeneracies of CB and VB first excited states ("CB 1P" and "HH 1P") are lifted by the coupling to remote bands. The same result was obtained for QD with C_{4v} geometry.[17] It is not related to atomistic, strain, or piezoelectric effects[5–7] but simply to the fact that the symmetry of the system in the eight-band description is represented by the $\boldsymbol{F}_z$ quantum number instead of the irreducible representations of the $C_{\infty v}$ symmetry group.

If the strain field is calculated using a continuum mechanical model (elasticity), the axial approximation (symmetry reduction from C_{4v} to $C_{\infty v}$) consists in defining an effective modulus $\bar{\boldsymbol{C}}$.[18]

Our approximation consists in replacing the elastic moduli $\boldsymbol{C}_{66}=\boldsymbol{C}_{44}$ by an effective modulus $\bar{\boldsymbol{C}}$ in the expression of the stress tensor obtained by an arbitrary rotation around the z axis. The elastic moduli are then the same for any frame chosen around the z axis,

$$\begin{pmatrix} \boldsymbol{C}'_{11} & \boldsymbol{C}'_{12} & \boldsymbol{C}_{12} & 0 & 0 & 0 \\ \boldsymbol{C}'_{12} & \boldsymbol{C}'_{11} & \boldsymbol{C}_{12} & 0 & 0 & 0 \\ \boldsymbol{C}_{12} & \boldsymbol{C}_{12} & \boldsymbol{C}_{11} & 0 & 0 & 0 \\ 0 & 0 & 0 & \boldsymbol{C}_{44} & 0 & 0 \\ 0 & 0 & 0 & 0 & \boldsymbol{C}_{44} & 0 \\ 0 & 0 & 0 & 0 & 0 & \bar{\boldsymbol{C}} \end{pmatrix},$$

with

$$\boldsymbol{C}'_{11} = \frac{\boldsymbol{C}_{11}+\boldsymbol{C}_{12}}{2} + \bar{\boldsymbol{C}}, \quad \boldsymbol{C}'_{12} = \frac{\boldsymbol{C}_{11}+\boldsymbol{C}_{12}}{2} - \bar{\boldsymbol{C}}, \quad \boldsymbol{C}'_{66} = \bar{\boldsymbol{C}},$$

and

$$\bar{\boldsymbol{C}} = \frac{\boldsymbol{C}_{11}-\boldsymbol{C}_{12}}{2} + \left(\boldsymbol{C}_{44} - \frac{\boldsymbol{C}_{11}-\boldsymbol{C}_{12}}{2}\right)\boldsymbol{d}.$$

This is a special case, with four independent parameters $(\boldsymbol{C}_{11},\boldsymbol{C}_{12},\boldsymbol{C}_{44},\bar{\boldsymbol{C}})$ of the "transverse isotropic" material type which corresponds to five independent parameters in the general case. This type of material is usually called "transverse isotropic." Notice that this approximation is much less restrictive than the "full isotropic" approximation usually proposed.[14] Our new proposition is also to use the components of strain tensor $\boldsymbol{\varepsilon}_{rr},\boldsymbol{\varepsilon}_{\varphi\varphi},\boldsymbol{\varepsilon}_{zz},\boldsymbol{\varepsilon}_{rz}$ adapted to cylindrical coordinates $(\boldsymbol{r},\boldsymbol{\varphi},\boldsymbol{z})$ instead of Cartesian ones,

$$\boldsymbol{\varepsilon}_{xx} = \cos^2(\varphi)\boldsymbol{\varepsilon}_{rr} + \sin^2(\varphi)\boldsymbol{\varepsilon}_{\varphi\varphi}, \tag{5}$$

$$\boldsymbol{\varepsilon}_{yy} = \sin^2(\varphi)\boldsymbol{\varepsilon}_{rr} + \cos^2(\varphi)\boldsymbol{\varepsilon}_{\varphi\varphi}, \tag{6}$$

$$\boldsymbol{\varepsilon}_{xz} = \cos(\varphi)\boldsymbol{\varepsilon}_{rz}, \quad \boldsymbol{\varepsilon}_{yz} = \sin(\varphi)\boldsymbol{\varepsilon}_{rz}, \tag{7}$$

$$\boldsymbol{\varepsilon}_{xy} = \frac{\sin(2\boldsymbol{\varphi})}{2}(\boldsymbol{\varepsilon}_{rr} - \boldsymbol{\varepsilon}_{\varphi\varphi}), \tag{8}$$

For bulk materials, the expressions of the acoustic velocities for various values of d are given in Table I. The best approximation of the cubic case is the transverse isotropic case with $d=0.5$, where acoustic velocities are angular averages of the corresponding cubic values.

When considering now the strained part of the 8×8 bulk Hamiltonian,[1] we propose also to introduce an axial approximation. This approximation will be applied for the R_ε term by analogy to the unstrained Hamiltonian,

$$R_\varepsilon = \frac{b\sqrt{3}}{2}(\varepsilon_{rr} - \varepsilon_{\varphi\varphi})\cos(2\varphi) - i\frac{d}{2}(\varepsilon_{rr} - \varepsilon_{\varphi\varphi})\sin(2\varphi). \tag{9}$$

In order to keep the 8×8 Hamiltonian in a block diagonal, we propose to replace in $\boldsymbol{R}_\varepsilon$ only, the coefficients containing the shear deformation potentials b and d by a mean value

$$\frac{\bar{\boldsymbol{b}}\sqrt{3}}{2} = \frac{1}{2}\left(\frac{\boldsymbol{b}\sqrt{3}}{2} + \frac{\boldsymbol{d}}{2}\right),$$

$$R_\varepsilon \approx \frac{\bar{\boldsymbol{b}}\sqrt{3}}{2}(\varepsilon_{rr} - \varepsilon_{\varphi\varphi})e^{-i2\varphi}. \tag{10}$$

This approximation is reasonable for the semiconductors considered in this study since these parameters are for InAs, $b\sqrt{3}/2=-1.58$ eV, $d/2=-1.80$ eV, for InP, $b\sqrt{3}/2=-1.73$ eV, $d/2=-2.50$ eV, and for GaAs, $b\sqrt{3}/2=-1.56$ eV, $d/2=-2.25$ eV. The other components of the strained Hamiltonian can be given in cylindrical coordinates without adding anymore approximations,

$$S_\varepsilon = -d\varepsilon_{rz}e^{-i\varphi}, \quad \boldsymbol{A}_\varepsilon = \boldsymbol{a}_c(\boldsymbol{\varepsilon}_{rr} + \boldsymbol{\varepsilon}_{\varphi\varphi} + \boldsymbol{\varepsilon}_{zz}),$$

$$\boldsymbol{P}_\varepsilon = \boldsymbol{a}_v(\boldsymbol{\varepsilon}_{rr} + \boldsymbol{\varepsilon}_{\varphi\varphi} + \boldsymbol{\varepsilon}_{zz}), \quad \boldsymbol{Q}_\varepsilon = \boldsymbol{b}\left(\boldsymbol{\varepsilon}_{zz} - \frac{\boldsymbol{\varepsilon}_{rr} + \boldsymbol{\varepsilon}_{\varphi\varphi}}{2}\right),$$

$$U_\varepsilon = \frac{-P_o}{\sqrt{3}}\frac{\hbar^2}{2m_0}(k_z\varepsilon_{zz} + k_i\varepsilon_{rz}),$$

$$V_\varepsilon = -\frac{1}{\sqrt{6}}\frac{\hbar^2}{2m_0}(P_o k_-\varepsilon_{rr} + P_o k_z\varepsilon_{rz}e^{-i\varphi}) \tag{11}$$

III. ELECTRONIC PROPERTIES

Figure 2(a) shows the variation of gap energy as a function of the truncation height (TH) for InAs/InP QD in the same conditions as the work performed in Ref. 3 (i.e., with a

TABLE I. General expressions of the longitudinal v_L and transverse v_{T1}, v_{T2} acoustic velocities for a bulk material along two directions of propagation, e.g., [001] and [110] in the (x,y) plane, for the full isotropic, $d=0$ and $d=1$ transverse isotropic, and cubic cases.

	[100]			[110]		
	v_L	v_{T1}	v_{T2}	v_L	v_{T1}	v_{T2}
Isotropic	$\sqrt{\frac{C_{11}}{\rho}}$	$\sqrt{\frac{(C_{11}-C_{12})}{2\rho}}$	$\sqrt{\frac{(C_{11}-C_{12})}{2\rho}}$	$\sqrt{\frac{C_{11}}{\rho}}$	$\sqrt{\frac{(C_{11}-C_{12})}{2\rho}}$	$\sqrt{\frac{(C_{11}-C_{12})}{2\rho}}$
$d=0$	$\sqrt{\frac{C_{11}}{\rho}}$	$\sqrt{\frac{(C_{11}-C_{12})}{2\rho}}$	$\sqrt{\frac{C_{44}}{\rho}}$	$\sqrt{\frac{C_{11}}{\rho}}$	$\sqrt{\frac{(C_{11}-C_{12})}{2\rho}}$	$\sqrt{\frac{C_{44}}{\rho}}$
$d=0.5$	$\sqrt{\frac{3C_{11}+C_{12}}{4\rho}+\frac{C_{44}}{2\rho}}$	$\sqrt{\frac{C_{11}-C_{12}}{4\rho}+\frac{C_{44}}{2\rho}}$	$\sqrt{\frac{C_{44}}{\rho}}$	$\sqrt{\frac{3C_{11}+C_{12}}{4\rho}+\frac{C_{44}}{2\rho}}$	$\sqrt{\frac{C_{11}-C_{12}}{4\rho}+\frac{C_{44}}{2\rho}}$	$\sqrt{\frac{C_{44}}{\rho}}$
$d=1$	$\sqrt{\frac{(C_{11}+C_{12})}{2\rho}+\frac{C_{44}}{\rho}}$	$\sqrt{\frac{C_{44}}{\rho}}$	$\sqrt{\frac{C_{44}}{\rho}}$	$\sqrt{\frac{(C_{11}+C_{12})}{2\rho}+\frac{C_{44}}{\rho}}$	$\sqrt{\frac{C_{44}}{\rho}}$	$\sqrt{\frac{C_{44}}{\rho}}$
Cubic	$\sqrt{\frac{C_{11}}{\rho}}$	$\sqrt{\frac{C_{44}}{\rho}}$	$\sqrt{\frac{C_{44}}{\rho}}$	$\sqrt{\frac{(C_{11}+C_{12})}{2\rho}+\frac{C_{44}}{\rho}}$	$\sqrt{\frac{(C_{11}-C_{12})}{2\rho}}$	$\sqrt{\frac{C_{44}}{\rho}}$

wetting layer thickness of 2 ML). This variation is presented for several values of d and also for the full isotropic case. The wetting layer energy is also shown on the top of the figure. A continuous decrease of the energy gap is predicted in good agreement with our previous full-3D study[3] and experimental results.[15,16] The variation of hydrostatic strain $\varepsilon_{hydro}=\varepsilon_{rr}+\varepsilon_{\varphi\varphi}+\varepsilon_{zz}$ (dotted line) and biaxial strain $\varepsilon_{biaxial}=\varepsilon_{rr}+\varepsilon_{\varphi\varphi}-2\varepsilon_{zz}$ (straight line) is represented for a vertical line passing through the center of a full cone. It indicates that the confining potentials (hydrostatic strain) for HH and CB are almost constant inside the conic QD, whereas LH potential is stabilized at the top of the cone thanks to the inverted biaxial strain.[3]

The variation of the "CB 1S" ($F_Z=\pm 1/2$)-CB 1P ($F_Z=\pm 1/2$ or $F_Z=\pm 3/2$) and "HH 1S" ($F_Z=\pm 3/2$)-HH 1P ($F_Z=\pm 1/2$ or $F_Z=\pm 5/2$) energy gaps are reported in Fig. 3(a) (the average values are considered for the first CB and HH excited states). A continuous increase of the energy difference between ground state and excited state is predicted for the CB with increasing TH. Indeed, the average radius is decreasing when increasing the TH for the chosen cone. In the VB, a maximum is reached for a TH equal to 7 ML. These results are also in good agreement with our previous work,[3] where the energy difference between ground and excited states has been attributed to the average QD radius, although no systematic study of this property was performed. When the TH is further increased, coupling between HH and LH bands (related to the gap increase [Fig. 2(a)] and the biaxial strain inversion [Fig. 2(b)] becomes more important than the decrease of the average radius.

Figure 3(b) shows the variation of the CB first excited state fine structure splitting $E_{F_z=\pm 3/2}-E_{F_z=\pm 1/2}$ ("1P splitting for electrons") as a function of the TH. This splitting predicted from symmetry considerations remains very small (less than 1 meV) and is related to the couplings of the "CB

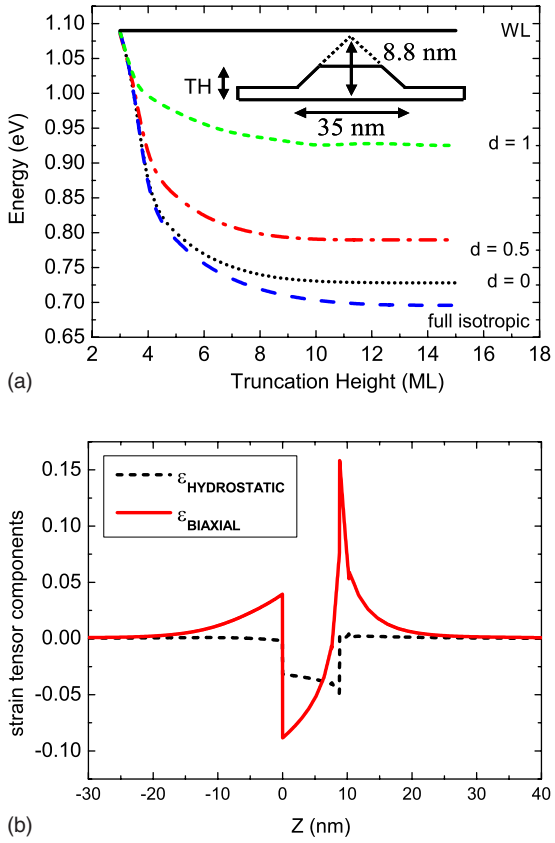

FIG. 2. (Color online) (a) Variation of the gap energy for $d=0$, 0.5, 0.75, and 1 and for the full isotropic case as a function of the truncation height (TH) for an InAs/InP QD. The wetting layer gap energy is also represented. (b) Variations of the hydrostatic strain $\varepsilon_{hydro}=\varepsilon_{rr}+\varepsilon_{\varphi\varphi}+\varepsilon_{zz}$ (dotted line) and the biaxial strain $\varepsilon_{biaxial}=\varepsilon_{rr}+\varepsilon_{\varphi\varphi}-2\varepsilon_{zz}$ (straight line) along a vertical line passing through the center of a full cone.

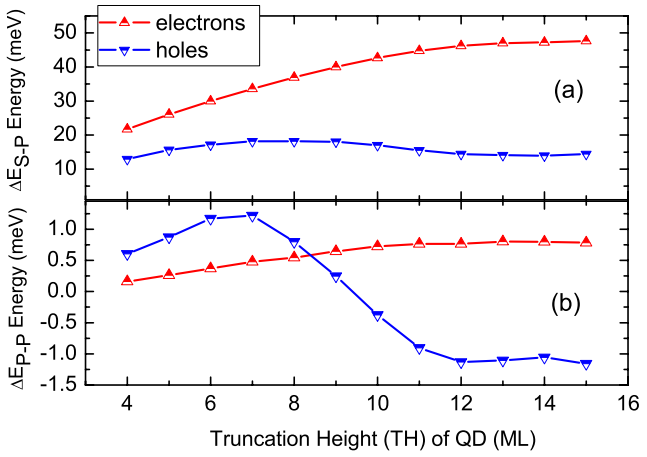

FIG. 3. (Color online) (a) Variations of the CB 1S-CB 1P (straight line) and HH 1S-HH 1P (dotted line) energy gaps as a function of the truncation height for an InAs/InP QD. (b) Variation of the CB and VB first excited state splittings, $E_{F_z=\pm 3/2}-E_{F_z=\pm 1/2}$ (straight line) and $E_{F_z=\pm 1/2}-E_{F_z=\pm 5/2}$ (dotted line) as a function of the truncation height for an InAs/InP QD.

1P" excited states to VB states, mainly HH states. This "1P-electrons" splitting increases as the energy gap decreases. In the case of the VB, the first excited state splitting $E_{F_z=\pm 1/2}-E_{F_z=\pm 5/2}$ ("1P splitting for holes") remains small and changes sign for a TH on the order of 8 ML. This is again associated with the strong increase of the HH-LH coupling.

We finally propose (Fig. 4) a comparison between the InAs/InP and the InAs/GaAs system with the same QD geometry (TH=2.9 nm). Due to the larger lattice mismatch in the InAs/GaAs case, a larger energy gap is found (0.90 eV for InAs/GaAs and 0.78 eV for InAs/InP). The same trend is observed for the calculated CB 1S-CB 1P (30.6 meV for InAs/GaAs and 26.2 meV for InAs/InP) and HH 1S-HH 1P (19.7 meV for InAs/GaAs and 16.2 meV for InAs/InP) energy gaps. As a result, the CB $E_{F_z=\pm 3/2}-E_{F_z=\pm 1/2}$ (0.14 meV for InAs/GaAs and 0.27 meV or InAs/InP) and VB $E_{F_z=\pm 1/2}-E_{F_z=\pm 5/2}$ (0.85 meV for InAs/GaAs and 0.95 meV for InAs/InP) splittings are smaller for the InAs/GaAs QD. Figures 4(a) and 4(b) represent, respectively, the isodensity surfaces containing 75% of the total density for the $\boldsymbol{F}_z=\pm 1/2$ CB ground state and the $\boldsymbol{F}_z=\pm 1/2$ CB first excited state (the difference with the CB $F_z=\pm 3/2$ first excited state is very small). It is straightforward to check that the spatial distribution of the electronic density has a cylindrical symmetry which is awaited for QD geometries corresponding to the $C_{\infty v}$ symmetry. It is possible to introduce a symmetry breaking by simulating the influence of the piezoelectric potential. Within our axial model, the linear piezoelectric polarization $\vec{\mathbf{P}}_1$ is equal to[18]

$$\vec{P}_1 = 2e_{14}\left[\sin(2\varphi)\varepsilon_{rz}\vec{u}_r + \cos(2\varphi)\varepsilon_{rz}\vec{u}_\varphi + \frac{\sin(2\varphi)}{2} \times(\varepsilon_{rr}-\varepsilon_{\varphi\varphi})\vec{u}_z\right]. \quad (12)$$

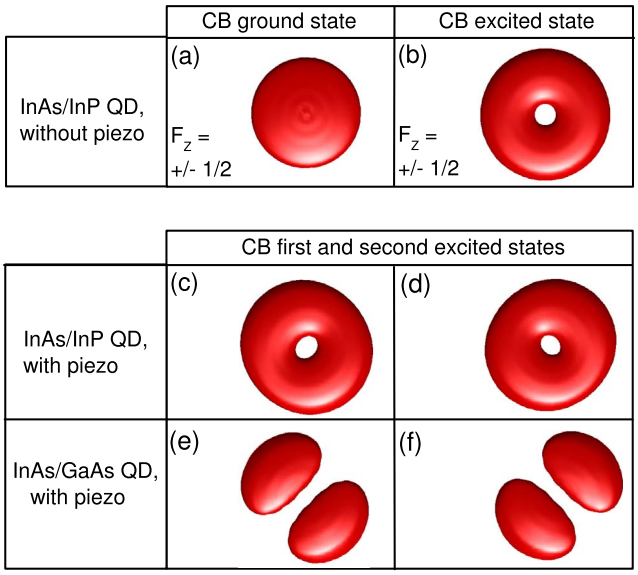

FIG. 4. (Color online) Comparison between the InAs/InP and the InAs/GaAs systems with the same QD geometry (TH =2.9 nm). The isodensity surfaces containing 75% of the total density are shown for the (a) $\boldsymbol{F}_z=\pm 1/2$ CB ground state and the (b) $\boldsymbol{F}_z=\pm 1/2$ CB first excited state in the InAs/InP QD. Isodensity surfaces containing 75% of the total density for the eigenstates (c) and (d) obtained after applying the piezoelectric potential as a perturbation to the $\boldsymbol{F}_z=\pm 1/2$ CB and $F_z=\pm 3/2$ CB first excited states in the InAs/InP QD. The same result is presented [(e) and (f)] for the InAs/GaAs QD.

The piezoelectric potential obtained after solving the Poisson equation is applied as a perturbation to the $\boldsymbol{F}_z=\pm 1/2$ CB and $F_z=\pm 3/2$ CB first excited states. The amplitude of the piezoelectric potential is small for the InAs/InP QD. The resulting states [Figs. 4(c) and 4(d)] show only a small deviation from the cylindrical symmetry. The perturbation was then applied to the same states in the InAs/GaAs QD. The C_{2v} symmetry clearly appears on Figs. 4(e) and 4(f). This is due to the smaller $E_{F_z=\pm 3/2}-E_{F_z=\pm 1/2}$ splitting but also to a larger piezoelectric field. This conclusion is not modified for this QD by the inclusion of the second order piezoelectric potential.[5–7,18] The second order polarization is calculated in the same way as in Eq. (1) of Ref. 7,

$$P_\mu = \sum_j \tilde{e}^0_{\mu j}\eta_j + \frac{1}{2}\sum_{jk}\tilde{B}_{\mu jk}\eta_j\eta_k, \quad (13)$$

where η is the strain in Voigt notation, and e and B are, respectively, the linear and nonlinear coefficients of the piezoelectric tensor.

Within our semianalytical approach, a simple expression is also obtained for the polarization related to this component,

$$\vec{P}_2 = \begin{cases} \sin(2\varphi)[2B_{114}(\varepsilon_{rr}+\varepsilon_{\varphi\varphi})\varepsilon_{rz} + 2B_{124}(\varepsilon_{rr}+\varepsilon_{\varphi\varphi}+\varepsilon_{zz})\varepsilon_{rz} + 2B_{156}(\varepsilon_{rr}-\varepsilon_{\varphi\varphi})\varepsilon_{rz}]\vec{\mu}_r \\ \cos(2\varphi)[2B_{114}\varepsilon_{\varphi\varphi}\varepsilon_{rz} + 2B_{124}(\varepsilon_{rr}+\varepsilon_{zz})\varepsilon_{rz}]\vec{u}_\varphi \\ \sin(2\varphi)[B_{114}(\varepsilon_{rr}-\varepsilon_{\varphi\varphi})\varepsilon_{zz} + B_{124}(\varepsilon_{rr}^2-\varepsilon_{\varphi\varphi}^2) + 2B_{156}\varepsilon_{rz}^2]\vec{\mu}_z. \end{cases} \quad (14)$$

IV. CONCLUSION

We have shown by comparison to our previous study[3] that accurate results can be obtained in the description of electronic properties of InAs/InP QD by introducing a few approximations to the strained 8×8 Hamiltonian. In a previous study,[5] it was shown that, in QD with $C_{\infty v}$ geometry, a splitting of the electronic P states result either from an interface effect,[5–7] a relaxation via the valence force field method[2,3,5] or a piezoelectric effect,[2,3,5] whereas continuum mechanics associated to effective mass models produces a vanishing splitting.[15] We show here that, in addition, there is a nonvanishing splitting due to the coupling with VB bands. This splitting which clearly appears here, because a continuum method and symmetry adapted functions are used, is however small, particularly in the InAs/GaAs system.

*Corresponding author; jacky.even@insa-rennes.fr

[1] T. B. Bahder, Phys. Rev. B **41**, 11992 (1990).
[2] O. Stier, M. Grundmann, and D. Bimberg, Phys. Rev. B **59**, 5688 (1999).
[3] C. Cornet, A. Schliwa, J. Even, F. Dore, C. Celebi, A. Letoublon, E. Mace, C. Paranthoen, A. Simon, P. M. Koenraad, N. Bertru, D. Bimberg, and S. Loualiche, Phys. Rev. B **74**, 035312 (2006).
[4] C. Cornet, F. Dore, A. Ballestar, J. Even, N. Bertru, A. Le Corre, and S. Loualiche, J. Appl. Phys. **98**, 126105 (2005).
[5] G. Bester and A. Zunger, Phys. Rev. B **71**, 045318 (2005).
[6] G. Bester, X. Wu, D. Vanderbilt, and A. Zunger, Phys. Rev. Lett. **96**, 187602 (2006).
[7] G. Bester, A. Zunger, X. Wu, and D. Vanderbilt, Phys. Rev. B **74**, 081305(R) (2006).
[8] P. Enders and M. Woerner, Semicond. Sci. Technol. **11**, 983 (1996).
[9] Calvin Yi-Ping Chao and S. L. Chuang, Phys. Rev. B **46**, 4110 (1992).
[10] Y. M. Mu and S. S. Pei, J. Appl. Phys. **96**, 1866 (2004).
[11] K. J. Vahala and P. C. Sercel, Phys. Rev. Lett. **65**, 239 (1990).
[12] P. C. Sercel and K. J. Vahala, Phys. Rev. B **42**, 3690 (1990).
[13] C. Pryor, Phys. Rev. B **57**, 7190 (1998).
[14] M. Tadic, F. M. Peeters, and K. L. Janssens, Phys. Rev. B **65**, 165333 (2002).
[15] P. Miska, J. Even, C. Paranthoen, O. Dehaese, A. Jibeli, M. Senes, and X. Marie, Appl. Phys. Lett. **86**, 111905 (2005).
[16] C. Cornet, M. Hayne, P. Caroff, C. Levallois, L. Joulaud, E. Homeyer, C. Paranthoen, J. Even, C. Labbe, H. Folliot, V. V. Moshchalkov, and S. Loualiche, Phys. Rev. B **74**, 245315 (2006).
[17] N. Vukmirovic, D. Indjin, V. D. Jovanovic, Z. Ikonic, and P. Harrison, Phys. Rev. B **72**, 075356 (2005).
[18] J. Even, F. Doré, C. Cornet, L. Pédesseau, A. Schliwa, and D. Bimberg, Appl. Phys. Lett. **91**, 122112 (2007).